Title	Antimony and antimony oxide@graphene oxide obtained by the peroxide route as anodes for lithium-ion batteries
Author(s)	Yu, Denis Yau Wai; Batabyal, Sudip Kumar; Gun, Jenny; Sladkevich, Sergey; Mikhaylov, Alexey A.; Medvedev, Alexander G.; Novotortsev, Vladimir M.; Lev, Ovadia; Prikhodchenko, Petr V.
Citation	Yu, D. Y. W., Batabyal, S. K., Gun, J., Sladkevich, S., Mikhaylov, A. A., Medvedev, A. G., et al. (2015). Antimony and antimony oxide@graphene oxide obtained by the peroxide route as anodes for lithium-ion batteries. Main group metal chemistry, 38(1-2), 43-50.
Date	2015
URL	http://hdl.handle.net/10220/25958
Rights	

Denis Y.W. Yu, Sudip K. Batabyal, Jenny Gun, Sergey Sladkevich, Alexey A. Mikhaylov, Alexander G. Medvedev, Vladimir M. Novotortsev, Ovadia Lev* and Petr V. Prikhodchenko

Antimony and antimony oxide@graphene oxide obtained by the peroxide route as anodes for lithium-ion batteries

Abstract: Zero-valent antimony and antimony oxide were deposited on graphene oxide by the recently introduced peroxide deposition route. The antimony@graphene oxide (GO) anode exhibits a charging capacity of 340 mAh g^{-1} with excellent stability at a current rate of 250 mA g^{-1} after 50 cycles of lithiation, which is superior to all other forms of antimony anodes that have been reported thus far. The electrode also exhibits a good rate performance, with a capacity of 230 and 180 mAh g^{-1} at a rate of 500 and 1000 mA g^{-1}, respectively. We attribute the superior performance of the antimony@GO anodes to our coating protocol, which provides a thin layer of nanometric antimony coating on the graphene oxide, and to a small amount of antimony oxide that is left in the anode material after heat treatment and imparts some flexibility. The efficient charge distribution by the large surface area of reduced GO and the expansion buffering of the elastic graphene sheets also contributed to the superior stability of the anode.

Keywords: antimony; antimony oxide; hydroperoxoantimonate; lithium-ion battery; reduced graphene oxide.

DOI 10.1515/mgmc-2015-0001
Received January 11, 2015; accepted February 16, 2015

***Corresponding author: Ovadia Lev,** The Harvey M. Krueger Family Center for Nanoscience and Nanotechnology and The Casali Institute of Applied Chemistry, The Institute of Chemistry, The Hebrew University of Jerusalem, Jerusalem 91904, Israel, e-mail: ovadia@mail.huji.ac.il
Denis Y.W. Yu: Energy Research Institute at NTU, Nanyang Technological University, 50 Nanyang Avenue, Singapore 639798, Singapore; TUM CREATE Centre for Electromobility, 1 CREATE Way, 10/F Create Tower, Singapore 138602, Singapore; and School of Energy and Environment, City University of Hong Kong, Tat Chee Avenue, Kowloon, Hong Kong SAR
Sudip K. Batabyal: Energy Research Institute at NTU, Nanyang Technological University, 50 Nanyang Avenue, Singapore 639798, Singapore
Jenny Gun: The Casali Institute of Applied Chemistry, The Institute of Chemistry, The Hebrew University of Jerusalem, Jerusalem 91904, Israel
Sergey Sladkevich: The Casali Institute of Applied Chemistry, The Institute of Chemistry, The Hebrew University of Jerusalem, Jerusalem 91904, Israel
Alexey A. Mikhaylov and Alexander G. Medvedev: The Casali Institute of Applied Chemistry, The Institute of Chemistry, The Hebrew University of Jerusalem, Jerusalem 91904, Israel; and Kurnakov Institute of General and Inorganic Chemistry, Russian Academy of Sciences, Leninskii prosp. 31, Moscow 119991, Russia
Vladimir M. Novotortsev and Petr V. Prikhodchenko: Kurnakov Institute of General and Inorganic Chemistry, Russian Academy of Sciences, Leninskii prosp. 31, Moscow 119991, Russia

Introduction

New generations of rechargeable batteries are essential for maintaining rapid momentum in the development of portable electronics and electric vehicles. Superior cathodes and electrolytes and new generations of large charge density anodes are gradually emerging. Great effort is being devoted to devising alternative lithium alloys such as tin, antimony, germanium, silicon and aluminum. Tin and particularly tin/carbon composites are by far the most promising alternative lithium-ion battery (LIB) anodes. However, antimony is also attracting significant attention due to its high theoretical charge capacity and its reasonable price. However, lithium alloying is often accompanied by a large volume change, which pulverizes the electrode upon repeated cycling and diminishes its performance attributes. Antimony lithiation to form Li_3Sb is associated with moderate volume expansion (147%), which is significantly lower than the volume change associated with, for example, tin expansion by $Li_{22}Sn_5$ formation (676%), though still much higher than the 9% volume change associated with graphite intercalation (Besenhard et al., 1990). Indeed, antimony-based electrodes, be they antimony oxide, zero-valent antimony or antimony sulfide, constitute attractive alternatives to the graphite lithium ion battery anodes. These materials have a theoretical capacity of 551, 660, and 946 mAh g^{-1}, respectively,

compared to the 372 mAh g^{-1} of graphite intercalation to form C_6Li. However, despite many efforts, the promise entailed in antimony and antimony oxide LIB anodes has never materialized. Lithium alloying by tin has proven to be much more successful than antimony lithiation.

The cyclability of lithium alloying was greatly improved by the introduction of carbon composites and later on by the introduction of reduced graphene oxide (rGO) composites. The latter provides an efficient, high surface area means to distribute the charge throughout the thick LIB anode, and its flexibility buffers large volume changes induced by lithiation and delithiation and thus minimizes electrode pulverization.

Several pathways to improve antimony oxide or antimony-based LIB anodes were examined. The deposition of antimony on mesoporous carbon supports was investigated by Chang (2008), who found approximately 100 mAh g^{-1} after 20 cycles. Zero-valent antimony on carbon with added cellulose showed some 100 mAh g^{-1} after 15 cycles (Caballero et al., 2008). Natural honeycomb-templated $LiSbO_3$ showed some 180 mAh g^{-1} (Kundu et al., 2011a). Although this was reduced by approximately 40–50% after 50 cycles, its performance was still much superior to the performance reported by those authors for non-templated $LiSbO_3$. $LiSbO_4$ was also proposed by Kundu et al. (2011b) but it exhibited a rather low average charge capacity (<100 mAh g^{-1}). Scorsati's group (Hassoun et al., 2008) showed a capacity of up to 200 mAh g^{-1} (at 100 mA g^{-1} charging rate) using approximately 500 nm antimony particles. Bryngelsson et al. studied electrodeposited antimony and antimony oxide films on nickel electrodes and showed remarkably high and stable LIB anode performance (Bryngelsson et al., 2007a,b). Over 600 mAh (g Sb)$^{-1}$ capacity was demonstrated for thin films of a mixture of antimony oxide and nanometric antimony deposited on etched nickel substrate.

Two other viable routes to exploit the high lithiation capacity of antimony should be mentioned in this introduction. We have recently demonstrated superior antimony sulfide LIB (Prikhodchenko et al., 2012; Yu et al., 2014) (and sodium ion battery; Yu et al., 2013) anodes by coating GO with a thin antimony sulfide layer that reached a specific capacity of 790 mAh g^{-1} after 50 cycles at 250 mA g^{-1}. Several authors have exploited the use of SnSb-graphene oxide and other bimetallic composites (Seng et al., 2011) and showed superior capacity compared to graphite, at least at moderate charging rates (Billaud et al., 2008; Simonin et al., 2008; Park and Sohn 2009; Chen et al., 2010; Fan et al., 2012; Jiang et al., 2012).

In a set of recent articles, we introduced the peroxide route for post-transition element coatings of graphene oxide and other particulates (Sladkevich et al., 2010, 2012a,b; Prikhodchenko et al., 2012). The hydroperoxide ligands regulate the polycondensation and aggregation in the aqueous solution, and due to being superior hydrogen donors (Prikhodchenko et al., 2011; Vener et al., 2011) (compared to hydroxo functionalities), they efficiently anchor nanoparticles to the solid oxide supports. In this study, we exploit the ability to produce ultrathin layers of nanoparticulate antimony oxide on reduced graphene oxide. Then we used another important feature that was introduced recently (Sladkevich et al., 2012a), namely the ability to reduce the metal oxide by high temperature reaction with the GO to form a zero-valent post-transition element deposit on the rGO. We show here that by controlling the high temperature treatment time, it is possible to obtain reduced graphene-oxide-supported nanometric crystalline antimony. Furthermore, we show that the crystalline antimony is coated by a thin antimony oxide layer. As a result of these two features, we obtain a very high specific charging capacity of reduced graphene-oxide-supported antimony LIB anodes.

Results and discussion

Characteristics of the active anode materials

Electron microscope imaging of the three coated graphenes, GO-Sb-80, rGO-Sb-300 and rGO-Sb-650 after heat treatment of peroxoantimonate@GO in vacuum at 80, 300 and 650°C, respectively, are depicted in Figure 1. The heat treatment distorted the flat graphene sheets, but other than that, it is difficult to notice the coatings on the GO. After treatment at 650°C, backscattered electron imaging revealed the emergence of 10–40 nm (antimony) dots on the graphene oxide. The large atomic number of antimony enhances the backscattering contrast.

The TEM images delineated in Figure 2 show gradual changes in the morphology of the active material. At room temperature, the material is by and large amorphous with the exception of tiny spots of crystalline cubic antimony (V) oxide that are probably formed at room temperature due to the local dismutation of the hydroperoxide functionalities and the evaporation of water. Tetramethylammonium hydroxide decomposes at high temperature, and the trimethylamine product evaporates as well. The d-spacing of the crystalline material is approximately 0.30 nm, which agrees well with the d_{222} spacing of cubic antimonic acid, i.e., hydrated Sb_2O_5, as described by Stewart et al. (1972).

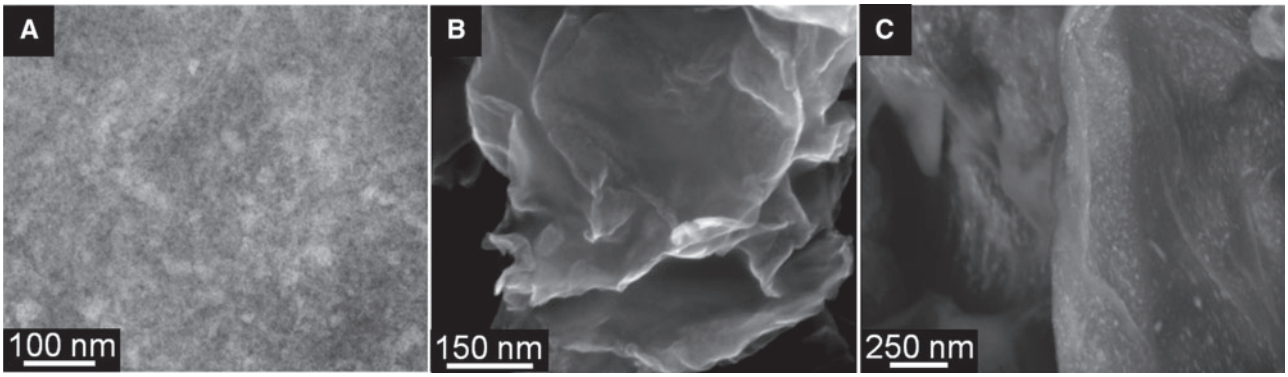

Figure 1: Scanning transmission electron microscope (STEM) images of heat-treated GO-supported antimony oxides: GO-Sb-80 (A), rGO-Sb-300 (B) and rGO-Sb-650 (C) in backscattering electron mode.

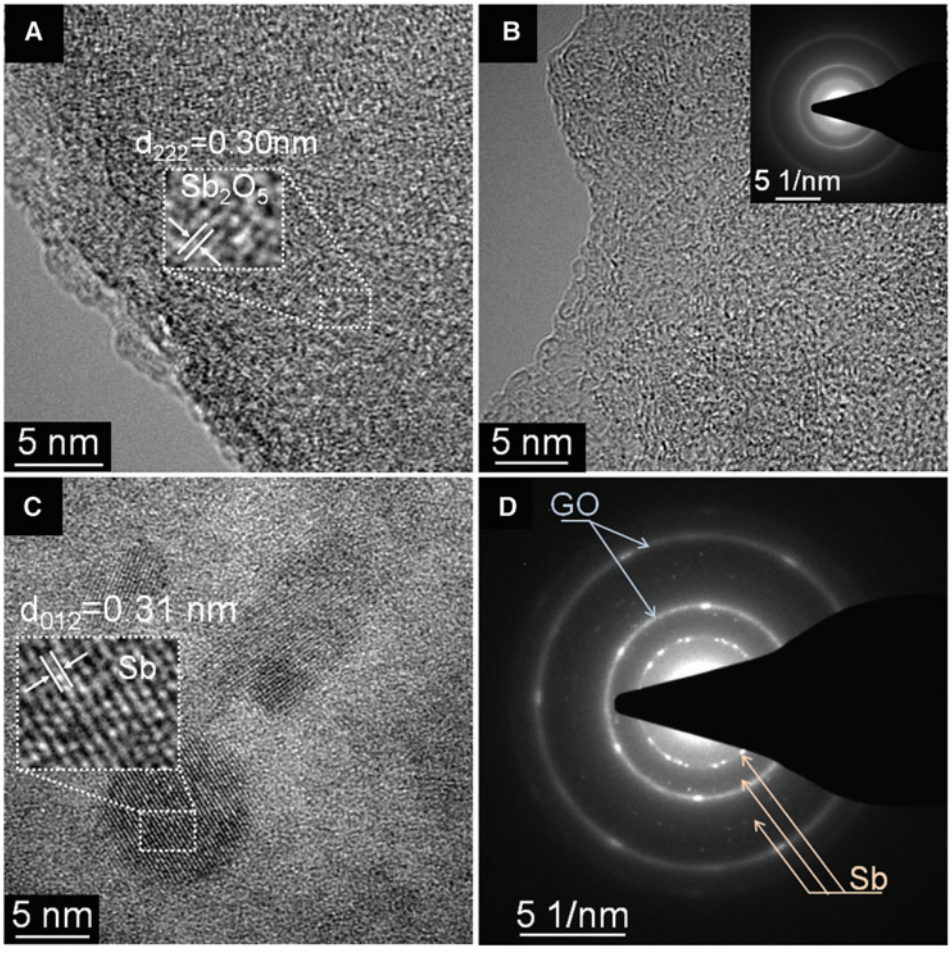

Figure 2: TEM images of antimony (V) oxide at room temperature with an insert that depicts nanocrystalline phases (A), rGO-Sb-300 (B) and rGO-Sb-650 (C).
The SAED of rGO-Sb-650 with the appropriate patterns of antimony (0) and GO are also shown in frame (D).

After heat treatment at 300°C, TEM imaging shows the formation of an amorphous coating that we interpret as antimony (III) oxide, rGO-Sb-300. After treatment at 300°C for a longer duration, or after heat treatment at 650°C for 2 h, crystallinity is observed (Figure 2C,D). Selected area electron diffraction (SAED) studies of the rGO-Sb-650 sample reflect the crystal structure of trigonal antimony(0). Additionally, the SAED pattern in Frame D of

Figure 2 shows the crystalline rings of the graphene oxide with d-spacings of approximately 2.1 Å and 1.2 Å, whereas the (002) peak of graphite with d-spacing of approximately 3.5 Å is absent altogether. Evidently, the coating hinders graphene stacking, and thus there is no long-range order in the z-direction. In addition to the dominant morphology that is depicted in Figure 2C, some spots of large trigonal antimony appear after 2 h of heat treatment at 650°C. Further heating at 650°C for 10 h did not change the TEM structure, but some larger crystals of antimony appeared, probably due to sublimation and recrystallization of the trigonal antimony phase.

The X-ray diffraction patterns in Figure 3 partially corroborate the electron microscopy conclusions. At room temperature, we observe minor crystallinity due to the antimony oxide hydrate. These nanocrystals, which are 3 nm according to the Scherrer equation, are destroyed at 80°C. Up to 300°C, the material is amorphous, but prolonged heating of the sample (e.g., for 2 h) at 300°C produces cubic (senarmontite) antimony oxide, which are 95 nm according to the Scherrer equation). We believe that the XRD powder diffraction is biased by some very small quantity of a large crystalline material that is obtained during heat treatment. It is important to minimize the duration of the heat treatment in order to prevent crystal growth. Indeed, in our previous publication on the heat-induced transformations of graphene-oxide-supported antimony oxide, we received mostly large crystals of antimony after 10 h of heat treatment at 650°C (Sladkevich et al., 2012a). More intensive heat treatment at 650°C gives the trigonal antimony phase (upper curve), with a crystallite size of 27 nm according to the Scherrer equation.

EDX studies revealed that the ratio between the antimony and the carbon support changes during heat treatment (Table 1). The O:C ratio goes from 1.4 at room temperature to 0.4 at 300°C due to a reduction of graphene oxide and antimony(V) oxide, and at a still higher temperature, the conversion from Sb(III) to Sb(0) reduces this ratio even further to 0.3. The Sb:C ratio is reduced from 2.1 to 0.9 after heat treatment due to sublimation, which becomes even more pronounced at higher temperatures, resulting in a Sb:C ratio of only 0.3 for the rGO-Sb-650 sample. The loss of antimony upon heat treatment is explained by the high vapor pressure of elemental antimony (above 10 Pa) at 650°C.

Surface area analysis by nitrogen adsorption reveals that the BET surface area (depicted in Table S1 in the Supplementary Material) increases gradually during the heat treatment and reaches over 300 m^2 g^{-1} for rGO-Sb-650. However, as discussed recently by Kuo et al. (2013), there is not necessarily a correlation between the specific surface area of the graphene oxide and their lithiation capacity as adsorption on specific functionalities plays a larger role than adsorption on defects or large surface areas.

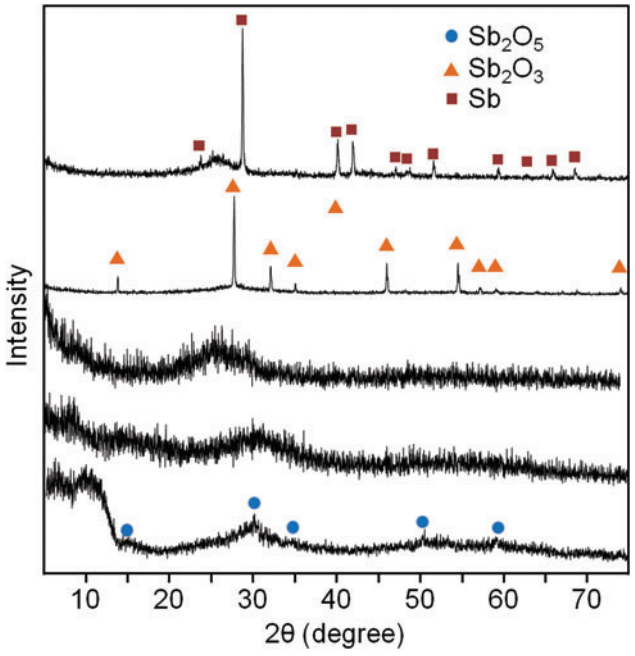

Figure 3: X-ray diffractograms of antimony oxide@GO. From bottom: Antimony oxide@GO at room temperature, after 5 h of heat treatment at 80°C, after 0.5 h at 300°C, after 2 h of heat treatment at 300°C and after 2 h of heat treatment at 650°C. The diffractions of cubic Sb_2O_5, cubic Sb_2O_3 and trigonal antimony (0) are indicated by circles, triangles and squares, respectively.

Electrochemical evaluation

The first charge and discharge profiles of GO-Sb-80, rGO-Sb-300 and rGO-Sb-650 are shown in Figure 4. All the electrodes show a first discharge capacity of >1000 mAh g^{-1}. The specific mass used for the calculation is the total mass of the rGO-Sb composite (i.e., 60% of the electrode mass).

Commercial Sb (Sigma Aldrich, 100 mesh) shows the typical profile with a discharge and charge plateau of approximately 0.87 V and 1.02 V, respectively. Discharge

Table 1: EDX elemental analysis of anode material.

Sample	Temperature/heat time	Sb:C:O, weight ratio
GO-Sb^V	25°C/-	2.09:1:1.41
GO-Sb-80	80°C/5 h	1.62:1:1.32
rGO-Sb-300	300°C/0.5 h	0.88:1:0.42
rGO-Sb-650	650°C/2 h	0.28:1:0.27

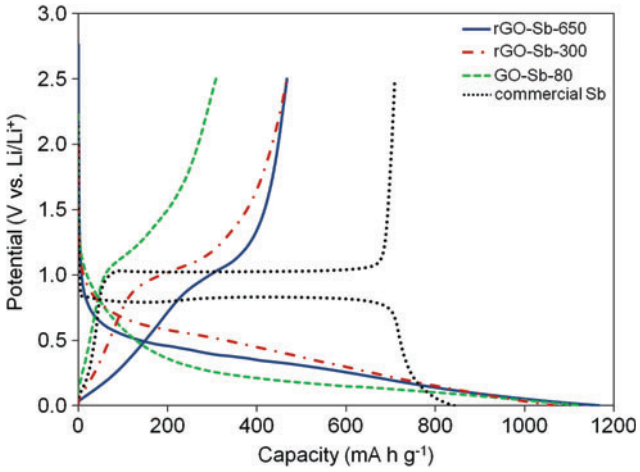

Figure 4: First-cycle charge and discharge profiles of different electrodes.

capacity is 843 mAh g^{-1} and charge capacity is approximatly 709 mAh g^{-1} with a first-cycle efficiency of 84.2%. Overall capacity is slightly higher than that of Li_3Sb formation, probably due to lithiation by the 20% carbon black in the electrode. Even though a large capacity can be obtained from the commercial Sb electrode, cycle performance is poor (see Figure 5A). Sb is expected to undergo a large volume change during alloying and de-alloying with Li, and the expansion and contraction of the material will lead to pulverization and loss of contact, resulting in loss in cycle capacity. The three graphene-oxide-supported electrodes, and particularly the two heat-treated electrodes, show good cycling stability, which is attributed to the reduction of the graphene at high temperature. The reduced graphenes are excellent electrical conductors, and thus they distribute the charge efficiently to the supported ultra-thin layers of antimony or antimony oxide. Additionally, the graphene contributes flexibility, which helps buffer volume changes and thus reduces electrode pulverization.

Cyclic voltammograms of the electrodes during the second cycle is shown in Figure 6. The two peaks corresponding to reductive lithiation to form Li_3Sb (0.59 V) and oxidative dealloying (1.10 V) can be seen. The Sb peak for the rGO-Sb-650 sample is smaller than that of rGO-Sb-300 due to the lower content of Sb in the material (Sb:C ratio of 0.3 for rGO-Sb-650 and 0.9 for rGO-Sb-300).

At a rate of 100 mA g^{-1}, the three electrodes GO-Sb-80, rGO-Sb-300 and rGO-Sb-650 show first charge capacities of 309, 467 and 468 mAh g^{-1}, respectively. The capacities of rGO-Sb-300 and rGO-Sb-650 are higher than the theoretical charging capacity of commercial graphite of 372 mAh g^{-1}. However, it should be noted that this comes at the expense of a lower operating potential of the cell as the average charging potential is 0.8 V, which is considerably larger than graphite. When the electrodes were cycled at 250 mA g^{-1}, all of them showed excellent stability, as compared to the commercial Sb electrode (see Figure 5A). Even though the initial capacity of the material is lower than that of the commercial Sb material, the stability makes up for the deficit.

The rate performance of the three antimony composites is shown in Figure 5B. Both charge and discharge rates are the same during each cycle. At a rate of 2000 mA g^{-1} (which is approximately 5C), the attainable capacity for rGO-Sb-650 is about 100 mAh g^{-1}. Because Sb has a reaction potential of around 0.8 V vs. Li/Li_+, the composite

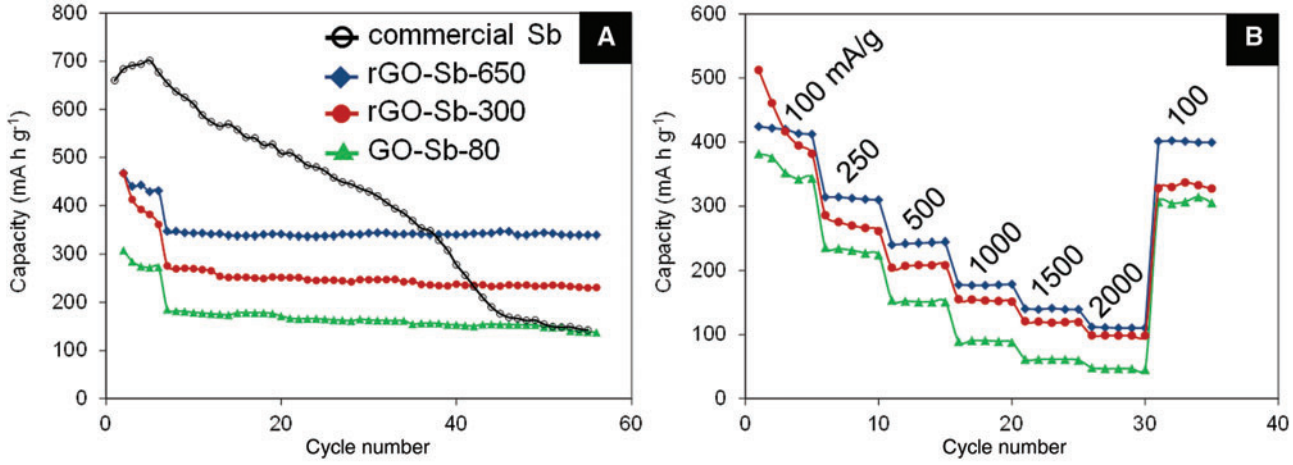

Figure 5: Cycle and rate performance of different antimony-based electrodes.
(A) Charging capacities of commercial antimony oxide (open circles), rGO-Sb-650 (diamonds), rGO-Sb-300 (closed circles) and GO-Sb-80 (triangles). The first five cycles were conducted at a current density of 100 mA g^{-1}, and the others at 250 mA g^{-1}. (B) Charging capacities of rGO-Sb-650, rGO-Sb-300 and GO-Sb-80 at different charging rates. The specific mass used for the calculation is the total mass of the rGO-Sb composite (i.e., 60% of the electrode mass).

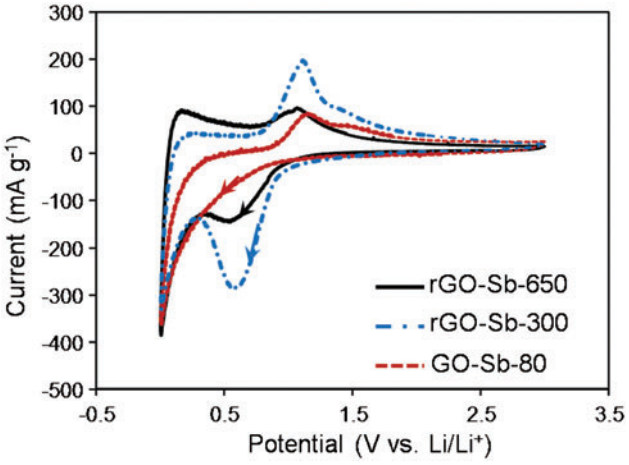

Figure 6: Cyclic voltammograms of the different electrodes during the second cycle.

can still give a considerable amount of capacity at a high charging rate (lithiation). In contrast, typical graphite anodes cannot be charged at 5C because the potential of the electrode will fall below the cut-off of 0 V, leading to safety concerns regarding Li dendrite formation.

The charge capacity of rGO-Sb-650 originates from both Sb and graphene. For comparison, Figure S1 (see Supplementary Material) shows the performance of a blank graphene oxide without Sb with the same electrode configuration and test range. The first charge capacity of rGO taken at a rate of 50 mA g^{-1} is 550 mAh (g graphene oxide)$^{-1}$, but the capacity decreases with cycling. However, after 35 cycles, the graphene blank electrode exhibited only approximately 270 mAh g^{-1} at a rate of 100 mA g^{-1}, whereas the rGO-Sb-650 exhibited a charge capacity of 410 mAh g^{-1} after 35 cycles at 100 mA g^{-1} (see Figure 5B showing cycling at different rates, but starting and ending at 100 mA g^{-1}).

The role of the morphology of Sb/C composite anodes was studied by Scorsati's group (Hassoun et al., 2008), who concluded that to increase the charge capacity, it would be necessary to reduce the size of the antimony particles to a few nm. Bryngelsson et al. (2007a,b), who studied electrodeposited antimony and antimony oxide films on nickel electrodes, concluded that three attributes are important to obtaining superior antimony-based LIB anodes: 1) Nanometric antimony particles are preferable; 2) thin film coatings function better; and 3) approximately 25% of antimony oxide improved electrode cyclability due to the formation of Li_2O volume buffering nano-grains. Whereas the thin film morphology condition was certainly satisfied in the rGO-Sb-300 and rGO-Sb-650, the best electrode was the rGO-Sb-650, despite its lower Sb content (Table 1). This electrode contained only antimony(0) according to our X-ray analysis (Figure 3) and TEM studies (Figure 2). To verify that there is no amorphous antimony oxide coating on the crystalline antimony particles, we have conducted XPS studies of the rGO-Sb-300 and rGO-Sb-650 samples (see Figure S2 in the Supplementary Material), and surprisingly, we observed that even after treatment at 650°C for 2 h, antimony (III) was the dominant antimony form and only a very small percentage of antimony (0) could be observed from the deconvoluted broad antimony binding energy peak. We have repeated the XPS analysis of the rGO-Sb-650 samples several times with different samples but received similar results. The XPS spectrum was in marked contrast to the X-ray and TEM studies, which showed only the presence of trigonal antimony (0) in the rGO-Sb-650 samples. We believe that the XPS results are biased by the large attenuation coefficient of the photoelectron emission of the thin coating of amorphous antimony oxide that is left after 2 h of 650°C heat treatment. Indeed, upon longer reduction (at 650°C for 10 h), the XPS spectra revealed reduction of all of the antimony to its zero-valent state (Sladkevich et al., 2012a). Thus, we believe that neither the XPS nor the X-ray diffractograms provide accurate quantitative composition data, and the combination of the two methods proves coexistence of antimony oxide and antimony (0) in the rGO-Sb-650 samples. Thus, in line with Bryngelsson's expectations based on electrochemical deposition studies, the best anodes contained a combination of antimony and antimony oxide phases.

Despite being inferior to the rGO-Sb-650 anode, the rGO-Sb-300 electrode also exhibited very good performance. The repeatability and stability were in fact superior to all previously reported antimony oxide electrodes. The charging capacity was 230 mAh g^{-1} after 50 cycles at a rate of 250 mA g^{-1}. We attribute the good performance of the rGO-Sb-300 (compared to previously reported carbon-coated antimony oxide electrodes) that was obtained by the peroxide deposition route to the thin amorphous coating that formed on the rGO. Several authors have already observed that amorphous films of lithiating hosts function better. For example, Xue et al. (2012) showed that amorphous germanium oxide LIB anodes exhibited much better performance compared to crystalline electrodes.

We believe that this article shows that antimony oxide and antimony-based LIB anodes are viable options. We also believe that this paper demonstrates the value of the peroxide synthesis route for obtaining high-performance, rGO-supported, antimony-based LIB anodes and thus provides additional evidence that the success of the peroxide deposition route is not confined to the production of rGO-supported SnO_2 and Sb_2S_3 LIB anodes that were previously reported (Prikhodchenko et al., 2012; Sladkevich et al., 2012b).

Conclusions

The evidence provided in this article can be divided into two levels. First, at the chemical synthesis/processing level, the article shows that the hydrogen peroxide synthesis route is a valuable (solution-based) technique for the production of a thin coating of antimony oxide@rGO and nanometric Sb(0)@rGO. This was demonstrated by the production of stable antimony-based LIB anodes. Second, the demonstration of a nanometric Sb(0)@rGO LIB anode with a high charge capacity and good stability confirms what numerous researchers before us have suspected but could not satisfactorily demonstrate: carbon-supported antimony and antimony oxide can be a viable alternative to the graphite LIBs.

Experimental section

Synthesis

Antimony and antimony-oxide-coated GO were synthesized by the peroxide route from a hydroxoantimonate precursor and a home-made GO, which was prepared by the modified Hummer's method (Zhou et al., 2009; Gun et al., 2012). First, a hydroxoantimonate precursor solution was obtained from aqueous $SbCl_5$, (99% purity, Sigma-Aldrich), and then peroxoantimonate-supported GO [GO-Sb(V)] was prepared, according to a methodology that was described in a recent publication (Sladkevich et al., 2012a), by dissolution of the hydroxoantimonate precursor solution in a basic hydrogen-peroxide-rich aqueous dispersion of GO (2 wt%). Selective precipitation of the peroxoantimonate on the GO was conducted by addition of a 1:1 ethanol:diethyl ether mixture acting as an anti-solvent. Details of the preparation protocols are provided in the online supplementary material.

Preparation of GO-Sb-80, rGO-Sb-300 and rGO-Sb-650

Heat treatment of the GO-Sb(V) powder was carried out in a tube furnace at 10^{-5} Pa pressure. The sample GO-Sb-80 was heated to 80°C for 5 h, the sample rGO-Sb-300 was heated to 300°C for 30 min and rGO-Sb-650 was heated to 650°C for 2 h. Additional heat treatments were conducted as delineated in the results section, but these samples were not evaluated as LIB anodes. Heating to the different set points was conducted at a rate of 0.8°C min^{-1} to prevent loss of the products by carryover.

Material characterization

Scanning electron microscopy (SEM and STEM), high resolution transmission electron microscopy (HRTEM), surface area BET studies, X-ray photoelectron spectroscopy (XPS) and X-ray powder diffraction (XRD) were conducted as detailed in the online supplementary material.

Electrochemical studies

Four antimony-containing samples were selected for electrochemical evaluation. Bulk crystalline Sb (Sigma-Aldrich) was used as is, and the materials denoted as GO-Sb-80, rGO-Sb-300 and rGO-Sb-650 were prepared as detailed above. In the following, we use the same nomenclature for the active electrode material and the anode that was made from it.

Electrochemical evaluation

Each of the different lithium intercalation materials was mixed with acetylene black and carboxymethylcellulose sodium salt (CMC, Sigma-Aldrich) in a weight ratio of 6:2:2, with deionized water as the medium to form a slurry. The slurry was then coated onto roughened copper foil as a current collector using a doctor blade. The electrode was dried at 80°C and pressed in a roll press. The electrodes were cut into 16-mm-diameter discs and further dried at 110°C for 4 h in vacuum before being introduced into an argon-filled glove box. The electrodes were assembled with Li metal as counter electrodes in a 2016 coin cell. As electrolyte, 1 M lithium hexafluorophosphate ($LiPF_6$) in an ethylene carbonate (EC) – diethyl carbonate (DEC) 1:1 solution was used. The cells were then tested with a battery tester (Neware) between 0 and 2.5 V vs. Li/Li^+. The typical charge-discharge rate was 100 mA g^{-1} during the first five cycles and 250 mA g^{-1} for subsequent cycles. The current rate used was typically 2.5 times higher than that reported for carbon-coated antimony electrodes in the literature. Cyclic voltammetry (CV) profiles were taken at a scan rate of 0.1 mV s^{-1} between 0.005 V and 3 V vs. Li/Li^+ (Biologic, VMP3). Rate performance was measured by testing the cell at current rates of 100, 250, 500, 1000, 1500 and 2000 mA g^{-1}.

Acknowledgments: This research is supported by the Singapore National Research Foundation under the CREATE programs TUM CREATE Centre for Electromobility and Nanomaterials for Energy and Water Management, by the Israel Ministry of Science and the Energy Research Institute at Nanyang Technological University. We thank The Harvey M. Krueger Family Center for Nanoscience and Nanotechnology of the Hebrew University of Jerusalem, the Israel Science Foundation and I-SAEF, Israel Strategic Alternative Energy Foundation for financial support. We thank the Russian Foundation for Basic Research (grant 14-29-04074). A.G. Medvedev thankfully acknowledges a Golda Meir Postdoctoral Fellowship and the Council on Grants of the President of the Russian Federation (SP-995.2015.1) for support. A.A. Mikhaylov thankfully acknowledges a Valazzi-Pikovsky Fellowship and the Council on Grants of the President of the Russian Federation (MK-5847.2014.3) for support.

References

Besenhard, J. O.; Hess, M.; Komenda, P. Dimensionally stable li-alloy electrodes for secondary batteries. *Solid State Ionics* **1990**, *40*, 525–529.

Billaud, D.; Nabais, C.; Mercier, C.; Schneider, R.; Wilimann, P. Electrochemical lithium insertion in graphite containing dispersed tin-antimony alloys. *Energy Conv. Manag.* **2008**, *49*, 2447–2454.

Bryngelsson, H.; Eskhult, J.; Nyholm, L.; Herranen, M.; Alm, O.; Edstrom, K. Electrodeposited Sb and Sb/Sb_2O_3 nanoparticle coatings as anode materials for Li-ion batteries. *Chem. Mater.* **2007a**, *19*, 1170–1180.

Bryngelsson, H.; Eskhult, J.; Edstrom, K.; Nyholm, L. Electrodeposition and electrochemical characterisation of thick and thin coatings of Sb and Sb/Sb_2O_3 particles for Li-ion battery anodes. *Electrochim. Acta* **2007b**, *53*, 1062–1073.

Caballero, A.; Morales, J.; Sanchez, L. A simple route to high performance nanometric metallic materials for Li-ion batteries involving the use of cellulose: the case of Sb. *J. Power Sources* **2008**, *175*, 553–557.

Chang, C. C. Sb-coated mesophase graphite powder as anode material for lithium-ion batteries. *J. Power Sources* **2008**, *175*, 874–880.

Chen, Z. X.; Cao, Y. L.; Qian, J. F.; Ai, X. P.; Yang, H. X. Antimony-coated SiC nanoparticles as stable and high-capacity anode materials for Li-ion batteries. *J. Phys. Chem. C* **2010**, *114*, 15196–15201.

Fan, S. F.; Sun, T.; Rui, X. H.; Yan, Q. Y.; Hng, H. H. Cooperative enhancement of capacities in nanostructured SnSb/carbon nanotube network nanocomposite as anode for lithium ion batteries. *J. Power Sources* **2012**, *201*, 288–293.

Gun, J.; Kulkarni, S. A.; Xiu, W.; Batabyal, S. K.; Sladkevich, S.; Prikhodchenko, P. V.; Gutkin, V.; Lev, O. Graphene oxide organogel electrolyte for quasi solid dye sensitized solar cells. *Electrochem. Commun.* **2012**, *19*, 108–110.

Hassoun, J.; Derrien, G.; Panero, S.; Scrosati, B. The role of the morphology in the response of Sb-C nanocomposite electrodes in lithium cells. *J. Power Sources* **2008**, *183*, 339–343.

Jiang, Q. L.; Xue, R. S.; Jia, M. Q. Electrochemical performance of Sn-Sb-Cu film anodes prepared by layer-by-layer electrodeposition. *Appl. Surf. Sci.* **2012**, *258*, 3854–3858.

Kundu, M.; Mahanty, S.; Basu, R. N. Improved electrochemical performance of natural honeycomb templated $LiSbO_3$ as an anode in lithium-ion battery. *Mater. Chem. Phys.* **2011a**, *130*, 20–23.

Kundu, M.; Mahanty, S.; Basu, R. N. Li_3SbO_4: a new high rate anode material for lithium-ion batteries. *Mater. Lett.* **2011b**, *65*, 1105–1107.

Kuo, S.-L.; Liu, W.-R.; Kuo, C.-P.; Wu, N.-L.; Wu, H.-C. Lithium storage in reduced graphene oxides. *J. Power Sources* **2013**, *244*, 552–556.

Park, C. M.; Sohn, H. J. A mechano- and electrochemically controlled SnSb/C nanocomposite for rechargeable Li-ion batteries. *Electrochim. Acta* **2009**, *54*, 6367–6373.

Prikhodchenko, P. V.; Medvedev, A. G.; Tripol'skaya, T. A.; Churakov, A. V.; Wolanov, Y.; Howard, J. A. K.; Lev, O. Crystal structures of natural amino acid perhydrates. *Cryst. Eng. Comm.* **2011**, *13*, 2399–2407.

Prikhodchenko, P. V.; Gun, J.; Sladkevich, S.; Mikhaylov, A. A.; Lev, O.; Tay, Y. Y.; Batabyal, S. K.; Yu, D. Y. W. Conversion of hydroperoxoantimonate coated graphenes to Sb_2S_3@graphene for a superior lithium battery anode. *Chem. Mater.* **2012**, *24*, 4750–4757.

Seng, K. H.; Guo, Z. P.; Chen, Z. X.; Liu, H. K. SnSb/graphene composite as anode materials for lithium ion batteries. *Adv. Sci. Lett.* **2011**, *4*, 18–23.

Simonin, L.; Lafont, U.; Kelder, E. M. SnSb micron-sized particles for Li-ion batteries. *J. Power Sources* **2008**, *180*, 859–863.

Sladkevich, S.; Mikhaylov, A. A.; Prikhodchenko, P. V.; Tripol'skaya, T. A.; Lev, O. Antimony tin oxide (ATO) nanoparticle formation from H_2O_2 solutions: a new generic film coating from basic solutions. *Inorg. Chem.* **2010**, *49*, 9110–9112.

Sladkevich, S.; Gun, J.; Prikhodchenko, P. V.; Gutkin, V.; Mikhaylov, A. A.; Medvedev, A. G.; Tripol'skaya, T. A.; Lev, O. The formation of a peroxoantimonate thin film coating on graphene oxide (GO) and the influence of the GO on its transformation to antimony oxides and elemental antimony. *Carbon* **2012a**, *50*, 5463–5471.

Sladkevich, S.; Gun, J.; Prikhodchenko, P. V.; Gutkin, V.; Mikhaylov, A. A.; Novotortsev, V. M.; Zhu, J. X.; Yang, D.; Hng, H. H.; Tay, Y. Y.; et al. Peroxide induced tin oxide coating of graphene oxide at room temperature and its application for lithium ion batteries. *Nanotechnology* **2012b**, *23*, 485601–485609.

Stewart, D. J.; Woodhams, F. W.; Knop, O.; Ayasse, C. Pyrochlores. VII. Oxides of antimony – X-ray and mossbauer study. *Can. J. Chem.* **1972**, *50*, 690–700.

Vener, M. V.; Medvedev, A. G.; Churakov, A. V.; Prikhodchenko, P. V.; Tripol'skaya, T. A.; Lev, O. H-bond network in amino acid cocrystals with H_2O or H_2O_2. The DFT study of serine-H_2O and serine-H_2O_2. *J. Phys. Chem. A* **2011**, *115*, 13657–13663.

Xue, D. J.; Xin, S.; Yan, Y.; Jiang, K. C.; Yin, Y. X.; Guo, Y. G.; Wan, L. J. Improving the electrode performance of Ge through Ge@C core-shell nanoparticles and graphene networks. *J. Am. Chem. Soc.* **2012**, *134*, 2512–2515.

Yu, D. Y. W.; Prikhodchenko, P. V.; Mason, C. W.; Batabyal, S. K.; Gun, J.; Sladkevich, S.; Medvedev, A. G.; Lev, O. High-capacity antimony sulphide nanoparticle-decorated graphene composite as anode for sodium-ion batteries. *Nat. Commun.* **2013**, *4*, 2922–2928.

Yu, D. Y. W.; Hoster, H. E.; Batabyal, S. K. Bulk antimony sulfide with excellent cycle stability as next-generation anode for lithium-ion batteries. *Sci. Rep.* **2014**, *4*, 4562.

Zhou, X. Z.; Huang, X.; Qi, X. Y.; Wu, S. X.; Xue, C.; Boey, F. Y. C.; Yan, Q. Y.; Chen, P.; Zhang, H. In situ synthesis of metal nanoparticles on single-layer graphene oxide and reduced graphene oxide surfaces. *J. Phys. Chem. C* **2009**, *113*, 10842–10846.

Supplemental Material: The online version of this article (DOI: 10.1515/mgmc-2015-0001) offers supplementary material, available to authorized users.